ELSEVIER

Journal of Hazardous Materials 140 (2007) 117–128

Journal of Hazardous Materials

www.elsevier.com/locate/jhazmat

Experimental study of the spill and vaporization of a volatile liquid

Douglas Bohl [a,*], Gregory Jackson [b]

[a] Department of Mechanical and Aeronautical Engineering, Clarkson University, Potsdam, NY, 13699, United States
[b] Department of Mechanical Engineering, University of Maryland, College Park, MD 20742, United States

Received 30 August 2005; received in revised form 7 April 2006; accepted 19 June 2006
Available online 27 June 2006

Abstract

Pool and vapor cloud characteristics of an acetone spill issuing from the downstream wall of a flow obstruction oriented perpendicular to a uniform flow were investigated experimentally. Data indicate that the spill event was largely governed by the temperature of the surface in relation to the boiling point of the spilled liquid. The free stream velocity (ranging from 0.75 to 3.0 m/s) also impacted the spreading of the spill. Planar laser-induced fluorescence (PLIF) was used to measure acetone vapor concentrations during the transient pool spreading and vaporization in a window 60 cm long by 50 cm high and located downstream of the 16 cm high obstruction. The recirculation region induced by the flow obstruction caused upstream transport of the acetone vapor along the spill surface, after which it was convected vertically along the obstruction wall before being entrained into the flow and convected downstream. The recirculating flow caused regions of vapor within the flammability limits to be localized near the flow obstruction. These regions moved into and out of the measurement plane by large three-dimensional flow structures. The flammable region of the evolved vapor cloud was observed to grow well past the downstream edge of the measurement domain. With decreasing wind speeds, both the mass of acetone vapor within the flammability limits and the total spill event time increased significantly. The data presented herein provides a basis for validating future spill models of hazardous chemical releases, where complex turbulent flow modeling must be coupled with spill spreading and vaporization dynamics.

Keywords: Vapor cloud formation; Liquid spill; PLIF; Flammability

1. Introduction

The number of tanker shipments of flammable liquids (both cryogenic and otherwise) has increased in recent years and with that, the potential for an accident involving a large spill and subsequent formation of a flammable or detonable vapor cloud. Understanding the potential hazards associated with liquid chemical spills is critical to the safe handling and transportation of these chemicals as well as for protection against intentional malicious acts. The potential hazard of the transportation of liquefied flammable chemicals has long been recognized. Fay [1] discussed the storage and transport of liquefied natural gas (LNG) and liquefied petroleum gas (LPG). Estimates of the risks associated with spills have been investigated, but in general, the complex coupling of the gas vapor dispersion with the liquid spill event, particularly in conjunction with convective air flows, has not been adequately addressed to provide reliable assessment for inputs of flammable vapor cloud size for explosion and fire models [2].

Model development efforts for spill and dispersion events have primarily been analytical and/or empirical in nature [3–5]. Typically, these models determine the size of the pool resulting from a spill at the point where gravity and inertial forces balance. They have generally included no coupling of the wind speed to the spill dynamics, thus neglecting the effects of viscous shear on the liquid spreading rate. This also limits their ability to be coupled to air flow models for subsequent mixing of fuel vapor with the surrounding air. A recent study extended these approaches to include complex multi-component vaporization [6] for LNG and LPG spills to assess how differences in species volatilities influence the liquid spill behavior. This study did incorporate the effects of wind upon the fuel evaporation rate by using a semi-empirical heat transfer coefficient as a function of wind speed, but the study did not look at the subsequent vapor-phase dynamics to assess how changes in gas-phase fuel vapor pressure due

* Corresponding author. Tel.: +1 315 268 6586; fax: +1 315 268 6695.
E-mail addresses: dbohl@clarkson.edu (D. Bohl), gsjackso@eng.umd.edu (G. Jackson).

0304-3894/$ – see front matter © 2006 Elsevier B.V. All rights reserved.
doi:10.1016/j.jhazmat.2006.06.076

to convective flows might influence vaporization. Nonetheless, the study did indicate that the vaporization rate could be over predicted by up to 20% if species were not accounted for in the evaporation model.

Spicer and Havens [7] investigated dispersion patterns of propane over a flat surface with two computational modeling codes, DEGADIS and FEM3A. While these models did not incorporate spill dynamics, the vapor-phase dispersion patterns were compared with an experimental study by Evans and Puttock [8]. Both codes predicted the general features of the experimental results indicating that windspeed and release rate primarily determined the amount of the fuel/air mixture within the flammability limits. However, because both of these models only consider the convective diffusive equations without allowing for transient turbulent structures, it remains uncertain as to the role of complex turbulent flow structures and mixing on this multi-component vaporization process.

Havens and Spicer [9] also investigated both experimentally and computationally the dispersion of dense flammable gases behind flow obstructions. This work targeted LNG spills from tanks into dike/impound enclosures designed to limit the spill to an area directly around the tank. Comparisons were made between FEM3A and scaled wind tunnel tests. In the experiments, propane doped with a tracer gas (CO_2) was released at a uniform rate to simulate a constant evaporation rate of LNG within the enclosure. The results show that a fuel air mixture within the lower flammability limits of LNG are found almost four tank diameters downstream of the enclosure. Further, the fluid flow around the tank creates regions on either side of the tank where the fuel/air mixture is within the flammability limits. This study differs from the current work in that the spilled liquid was contained and the pool size limited to the enclosure area.

In general, the effects of flow on the spill spreading, evaporation, and subsequent cloud formation remain uncertain. There is a general lack of experimental results to support the development of a spill and evaporation model. This limits the ability of current models to provide reliable risk assessment when it comes to large-scale releases of volatile liquid fuels.

The current study begins to address that lack by looking experimentally at a characteristic geometrical configuration and exploring the effect of wind and large-scale motions caused by flow obstructions on volatile liquid spills and subsequent cloud formation. In particular, this study imposed a uniform approach flow over a perpendicular obstruction, large with respect to the boundary layer, and with a downstream liquid release on the backside of the obstruction as illustrated in Fig. 1. A significant recirculation region will extend approximately six times the height of the obstruction downstream from the obstruction [10,11]. Fluid in this region can be trapped by the recirculating flow, and thus liquid spills of volatile fuels in the recirculation region can potentially result in the build up of a large flammable and detonable vapor clouds. The current study investigated this potential in a wind tunnel by spilling acetone onto a heated plate with a controlled temperature (or superheat with respect to the acetone boiling point). The scenario investigated was intended to represent a first order model of the spilling of a flammable liquid from the side of a tanker onto a liquid surface.

Two phases of this problem were investigated in this work: (1) the dynamics of the spill of the liquid onto the surface and (2) the dynamics of the vaporized chemical cloud. Measurements were taken of the maximum spill pool size, the lifetime of the spill pool, and its rate of evaporation. Both the wind speed and the surface temperature were independently controlled to investigate functional relationships of the various parameters. The subsequent concentration, size, and motion of the vapor cloud were also quantified. The objectives of these measurements were (1) to gain a better understanding of the spill and dispersion dynamics in the wake of an object that is large in comparison to the boundary layer, and (2) to provide benchmark experimental data with well defined boundary conditions for validation of computer spill and dispersion models given the limitations of laboratory scaled experiments for this scenario.

2. Experimental facility/methods

2.1. Facility

To provide controlled flow in an enclosed facility for safety, a low speed wind tunnel as illustrated in Fig. 1 was built and installed in the Shock Physics Facility at the Naval Surface Warfare Center's Indian Head Division. Due to the limited facility size an L-shaped wind tunnel was designed as shown. The settling chamber was pressurized by the flow from the fan. Outflow into the test section was conditioned first by screens within the settling chamber. Half-round pieces were placed at the entrance to the conditioning section and were followed by honeycomb and two sets of screens prior to the entrance of the test section. The test section of the wind tunnel was 76 cm × 76 cm × 122 cm long. Winds in the range of 0–5 m/s were generated using Continental 1 HP fan (Model # APK 240) with a variable frequency ac speed controller. The velocity varied linearly with controller frequency and was uniform to within 5% of the mean value across the test section as illustrated in Fig. 2. The RMS level of the free stream speed was less than 1% of the approach free stream speed, u_{in}.

The bottom of the test section was a machined aluminum plate with strip heaters mounted underneath the plate for heating. The

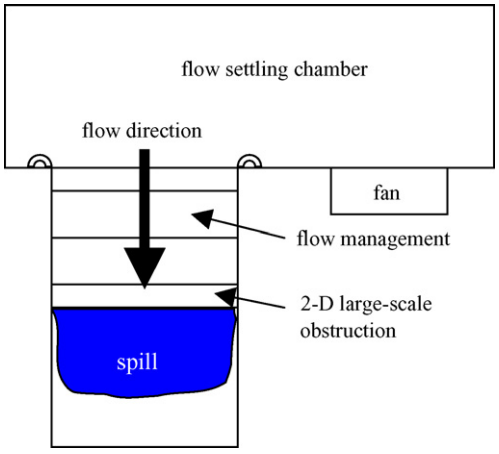

Fig. 1. Top view schematic of the dispersion test facility.

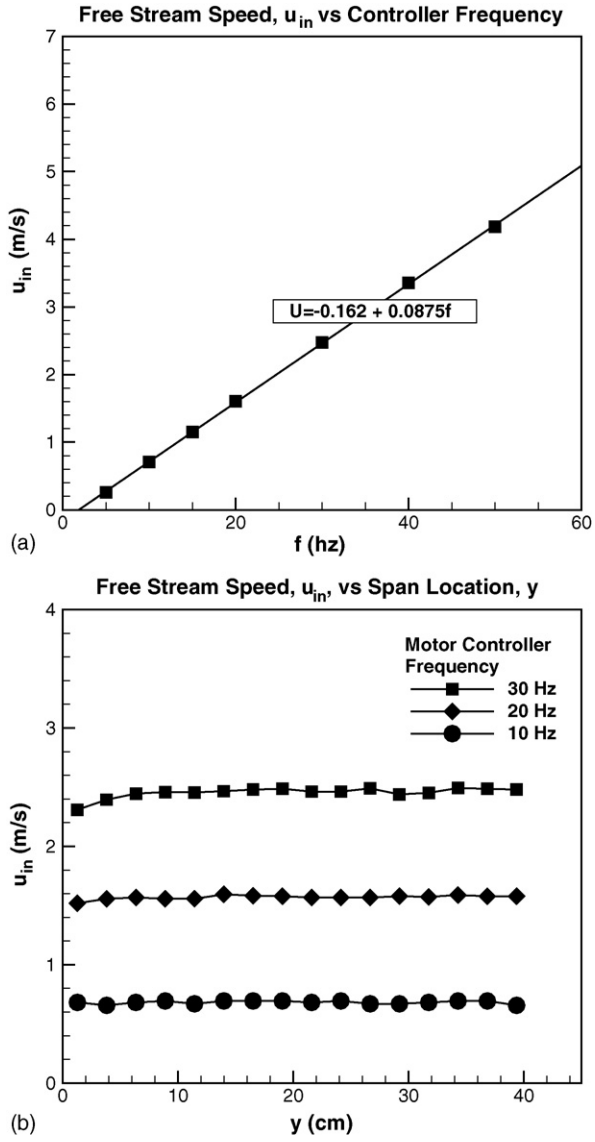

Fig. 2. (a) Free stream speed as a function of controller frequency. (b) Velocity profile across the test section. Free stream turbulence level <1% of the approach speed.

exposed top side of the aluminum plate was instrumented with 3.2 cm o.d. sheathed ungrounded thermocouples embedded into machined slots in the plate which were potted such that the surface was smooth. ac variacs controlled with PID temperature controllers using the surface mounted thermocouples provided power to the strip heaters along the base of the aluminum plate. The ac variacs were set at voltages so as to minimize oscillations in surface temperatures by reducing on–off switching of the heating power by the controllers. On the heated plate, a rectangular obstruction, 15.2 cm high × 10.2 cm wide, was fixed near the upstream edge of the test section. The obstruction spanned the cross-wise direction of the test section so as to avoid end-wall effects of the obstruction.

The liquid spill was simulated with a Cole–Parmer Micropump gear pump with an Ismatec programmable 0.2 hp digital drive (Model MCP-Z). The gear pump was able to provide a range of flows from 0.03 to 3.0 l/min. The programmable drive and the gear pump provided rapid start-up (<0.5 s) and rapid shut down (<1.0 s). The spill was issued through a 0.63 cm hole located 10.2 cm above the plate surface on the downstream wall of the obstruction in the central plane of the test section. The spill rate was held constant at the 1.68 l/min (28 cm^3/s), which provided a spill exit velocity u_{sp} = 88 cm/s. At this velocity, the spill showed slight separation from the wall such that the liquid jet landed on the plate approximately 3–4 cm away from the base of the obstruction.

2.2. Experimental methods

Several optical methods exist to measure species concentration in a gaseous flow field, but very few provide the ability to make planar measurements over the domain of interest in the current study. In this work, planar laser-induced fluorescence (PLIF) with its ability to provide a large measurement window was employed to quantify the species concentration of the chemical (acetone) as it evaporated. For acetone PLIF, the fourth harmonic (wavelength 266 nm) of an Nd-YAG laser can be used to excite the acetone such that it fluoresces as illustrated in the sample image in Fig. 3(a). The emitted light is imaged and the intensity is proportional to the concentration of the excited species, in this case acetone. If a reference intensity from a known concentration of the species can be measured and the imaging device remains within its linear region, then the concentration of the species can be fairly well quantified by knowing the local laser strength as shown in Fig. 3(b). More details on how to analyze PLIF images are discussed in previous references [12,13].

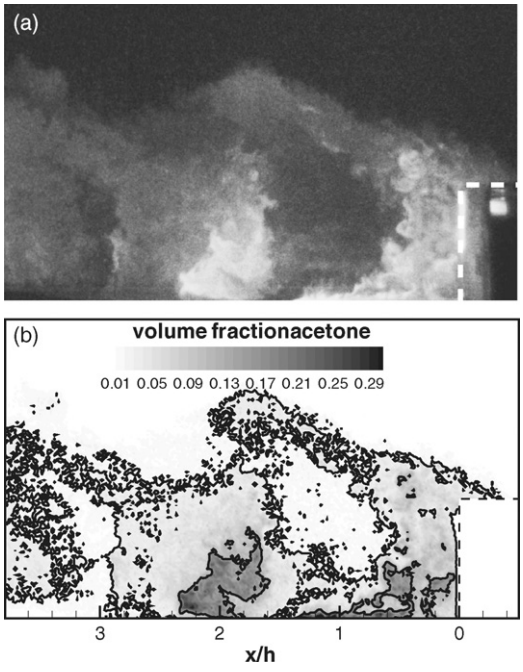

Fig. 3. (a) Sample PLIF image with nonlinear scaling to highlight regions of low concentration and (b) calculated concentration field. u_{in} = 3.0 m/s; T_p = 60 °C; V_{sp} = 250 ml. Acetone flammability limits (2.5 and 12.8% by volume) bounded in (b) by solid contour lines. Flow obstruction shown by dashed lines in both (a) and (b).

In this work, a Spectra Physics Quanta-Ray Pro 270-10 Nd-YAG pulsed laser was used as the light source to excite the acetone vapor. The Pro 270-10 provides approximately 150 mJ per pulse in the fourth harmonic at 266 nm with a pulse width of 3 ns. Cylindrical optics were used to create a two-dimensional sheet of laser light that was directed through the vapor cloud along the central plane of the wind tunnel. The fluorescence emitted by the acetone was captured via an intensified CCD camera (Cooke Corporation DiCam Pro). The reference concentration for each image was provided by a cell, the rectangular region contained within the flow obstruction in Fig. 3(a), filled with a known acetone concentration.

Acetone is widely used in gas-phase PLIF experiments and is therefore well characterized for these experiments [12,13]. Two properties, partial pressure and quantum efficiency for fluorescence determine the signal strength and therefore dynamic range of the concentration measurements. The relatively high saturation pressure of acetone, 180 Torr at 20 °C and its high quantum efficiency at the available laser wavelength translate into high signal to noise ratios and good dynamic range. The density of acetone vapor is twice that of air, which mimics chemicals of interest such as naphtha-like hydrocarbons. In particular, the molecular weight of acetone (MW = 58) matches that of butane, a common constituent of LPG. However unlike butane, acetone is a liquid at room temperature and has a boiling point of 56 °C. Thus, to offset the difference in volatilities of acetone and its similarly weighted hydrocarbon analogs, the surface of the spill in the wind tunnel was heated to various temperatures (up to 60 °C) to simulate rapid evaporation of the fuel.

The accuracy of a quantitative PLIF measurement is dependent upon knowing the concentration, the shot to shot energy variation in the laser beam, the spatial distribution of the beam energy, and the local beam attenuation. In this work, the reference concentration was known from the reference cell for each image, which also allowed the shot to shot variation in beam intensity to be accounted for in the calculations. Beam attenuation due to absorption by the fuel species is not typically accounted for when using acetone as a chemical tracer because attenuation is often negligibly small. However in this work, the beam passed through the downstream end of the tunnel and traveled through a long region of the test section, which included some acetone vapor convected downstream. Beam attenuation thus depended upon the experimental conditions and was indirectly accounted for by using the reference cell, whose intensity was also impacted by the beam attenuation. It was assumed that the attenuation in the 60 cm long measurement region was minimal, and thus, the attenuation at the cell location was comparable to the attenuation throughout the image. The last issue in quantifying the PLIF images is the spatial variation in the beam energy. In order to get the beam to illuminate the measurement region cylindrical lenses were used to spread the beam. A collimated beam was not possible because of the large beam height (50 cm). Therefore, there was spatial variation in the beam energy along the length of the laser sheet due to beam spread. This effect was not incorporated in the image post-processing, but the beam spreading angle of 5° only led to a decrease in beam strength over the distance of the measurement window of 5%.

The experimental set-up allowed multiple parameters to be investigated. The obstruction orientation was fixed with the long axis spanning the width of the tunnel. Experimental conditions were varied as follows: free stream speed, $u_{in} = 0$, 0.75, 1.5 and 3.0 m/s; plate temperature, $T_p = 20$, 40 and 60 °C; spill volumes, $V_{sp} = 125$ and 250 ml—which at the fixed spill rate accounted for spills of 5 and 10 s, respectively.

2.3. Experimental scaling issues

The motivational scenario, a liquid spill from a tanker onto a water surface, poses significant experimental issues that must be addressed in a laboratory study. The problem is governed by two non-dimensional parameters, the Reynolds ($Re = u_{in}h/\nu$) and Froude ($Fr = u_{in}/(gh)^{1/2}$) numbers. In this problem the length scale was taken to be the height of the flow obstruction while the velocity is taken was the approach speed. To accurately scale the problem both *Re* and *Fr* should be matched between the experiment and the full-scale scenario. Because of experimental facility limitations, gases other than air could not be used and therefore *Re* is dependant on u_{in} and *h* for scaling as is *Fr*. Investigation of the parameter definitions however shows that $Re \sim h$ while $Fr \sim h^{-1/2}$ therefore both *Re* and *Fr* cannot be matched simultaneously in the experiment.

The *Re* and *Fr* numbers can be estimated for typical environmental conditions. With a 5 m/s wind and a 10 m high tanker $Re = 6.8 \times 10^6$ and $Fr = 0.50$. Laboratory experimental conditions yield $Re = (0.8–3) \times 10^4$ and $Fr = 0.61–2.5$. In the experiment the speed was chosen to ensure a *Re* high enough to generate unsteady turbulent separation over the flow obstruction while also providing a *Fr* number near to the environmental condition. In the present experiments, the lowest u_{in} (0.75 m/s) matches the full-scale *Fr* for a 10 m tanker with a wind speed of 6 m/s. The higher u_{in} in the experiments result in an $Fr > 1$. One can expect therefore that there may be differences between the dynamics of the experiment and full-scale scenario, but the comparable *Fr* implies that the fluid physics are such that the obtained data can be used for validation of numerical codes.

Another significant difference between the experiment and a possible full-scale scenario is in the spill surface. A liquid spill onto a water surface will include complex dynamic phenomena such as distortion of the water surface, entrainment of atmospheric gasses, and potentially phase change of the water surface for cryogenic liquid spills. The extent of these effects is governed by the height and rate of the spill from the tanker. Because of analytical tractability, models of spills on liquid surfaces have generally treated the water surface as a flat, non-distorting interface [5,6]. In these experiments the aluminum surface provides a well defined boundary condition for model validation.

3. Results/discussion

3.1. Spill characterization

Fig. 4 shows still images from a typical spill characterization experiment. The spill event can be characterized by three stages. During the first phase ($t \approx 1–5$ s) the chemical marker was

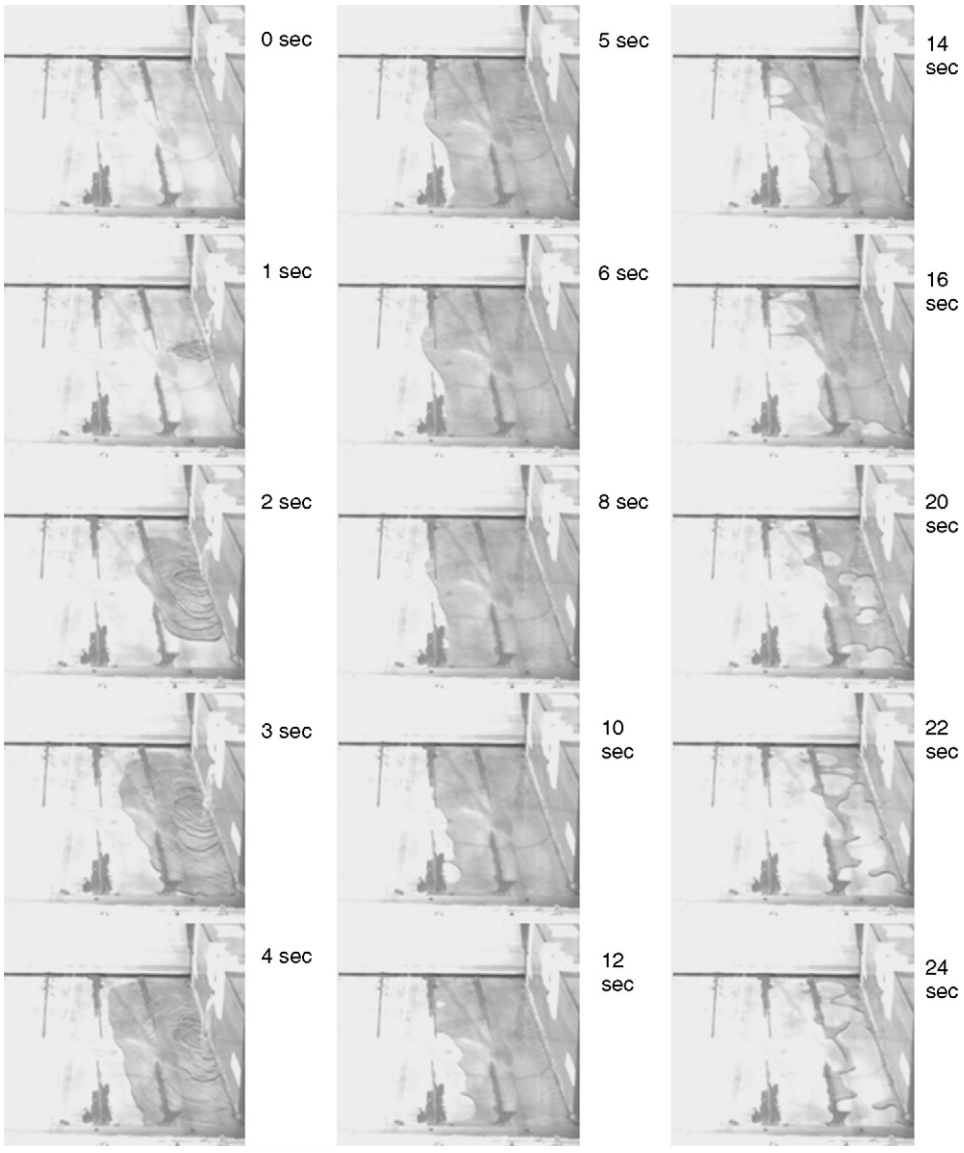

Fig. 4. Images of a typical spill characterization experiment. $V_{sp} = 125$ ml; $T_p = 60\,^{\circ}$C; $u_{in} = 3.0$ m/s. The flow direction in the images is right to left (i.e. the spill is on the downwind side of the obstruction).

released. The spill area increased both in the downstream and span-wise directions. The lateral spreading rate was typically three times faster for the spill than the stream-wise spreading rate and was uniform in both span directions. During the second phase ($t \approx 5$–8 s), the resulting pool maintained a near constant size, before entering the third phase ($t > 8$ s), where the size of the spill pool decreased due to evaporation and downstream dispersion. The PLIF images indicated that acetone was evaporated and dispersed through all three phases of the spill.

The spill event can be characterized by the maximum spill downstream distance, x_{max}, the time of constant spill size, t_c, and the regression speed of the spill downstream edge, u_{de}. Fig. 5 shows a trajectory map of the spill downstream edge for two different spill volumes with constant free stream speed and plate temperature. The downstream edge regression speed was indicated for the third phase of the spill during which the spill size decreased.

Fig. 6 shows the maximum downstream location of the spill as a function of the spill volume, plate temperature, and free stream speed. It is important to note that the data presented in this work come from a single realization for each case and as a result the error in each data point can be significant and detailed trends may not be reliable from these data. However, general trends can be described. The maximum spill size clearly increased with increased spill volume as expected though the maximum spill size did not double when the spill volume was doubled, Fig. 6(a). During the spill the acetone spread both downstream and laterally as was shown in Fig. 4. The laterally spread acetone reached a gutter on the edge of the test section and excess acetone spilled into the gutter which made it difficult to characterize the maximum spill area as quoted in several spill models. However, these models are based on the assumption of a radial spreading of the pool. The current flow configuration clearly showed a more rapid, nominally three times faster,

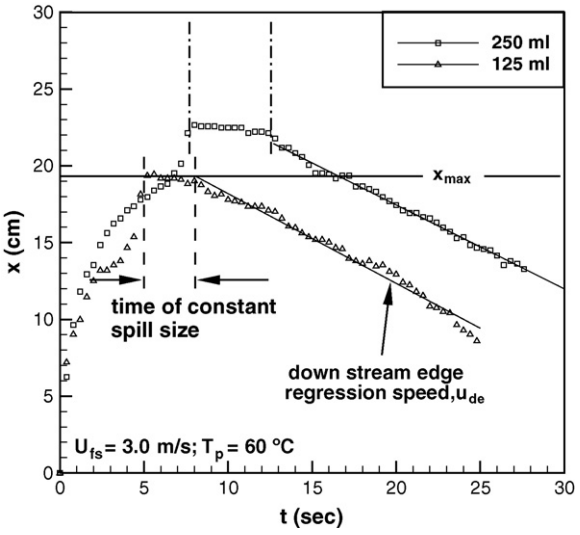

Fig. 5. Spill downstream edge trajectories as a function of time. $V_{sp} = 125$ ml; $T_p = 60\,^{\circ}$C; $u_{in} = 3.0$ m/s.

lateral spreading than downwind spreading. The reduced downwind spreading arises from the reverse flow downwind of the obstruction, which enhanced the lateral spreading of the spill. There was no clear trend in the maximum spill size as a function of free stream wind speed, Fig. 6(b). On the other hand, there was a clear function with plate temperature. As shown in Fig. 6(c), the spill size decreased by approximately 25% when the plate temperature was raised from room temperature to 60 °C (4 °C above the boiling point of acetone). Such an increase in plate temperature had as significant an effect on the spill size as halving the liquid spill volume. Thus, accurate heat transfer models are critical for predicting both spill and dispersion dynamics.

Determining the rate at which the spilled pool shrank in the third phase of the spill provided an indirect measure for the vaporization rate. As shown in Fig. 5, the slope of the downstream regression rate u_{de} was plotted versus the experimental parameters and the results are shown in Fig. 7. There was no dependence observed for u_{de} on the total spill volume, which indicated that once the pool was heated to the vaporization point pool size did not play a significant role in determining the evaporation rate. This also suggests that the spill thickness was probably similar for the two spill volumes. A clear dependence in u_{de} was observed for the plate temperature and free stream speed as indicated in Fig. 7(b) and (c), respectively. Increasing the free stream speed increased the regression and evaporation rate suggesting the importance of heat and mass transfer on pool evaporation. The dependence was nominally linear and independent of the spill volume over the wind range investigated. In the absence of any flow the evaporation of the acetone on the plate proceeded until the gas-phase concentration of acetone approached its saturated value above the plate as indicated in Fig. 8. As the saturation pressure was approached the rate of vaporization is limited by the diffusion of the vapor into the surrounding air. The higher MW of acetone than that of air tended to suppress buoyancy-driven flows that might otherwise arise

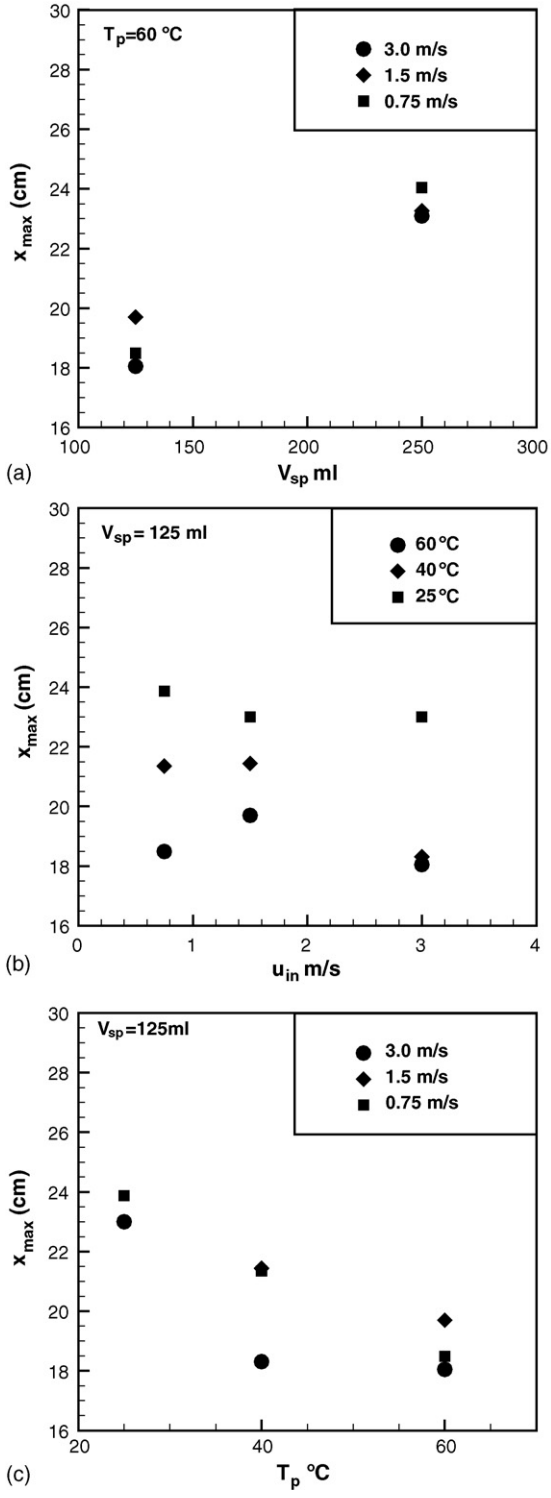

Fig. 6. Maximum spill size, x_{max}, as a function of (a) spill volume V_{sp}, (b) free stream speed u_{in} and (c) plate temperature T_p.

from the heated plate and thus, there was no strong evidence of buoyancy-driven mixing above the dense acetone layer near the plate in Fig. 8. As free stream velocity increased from the zero velocity condition, augmentation of diffusion by gas-phase convection caused an increase in vaporization rates as indicated by the rise in u_{de} with u_{in} in Fig. 7(b).

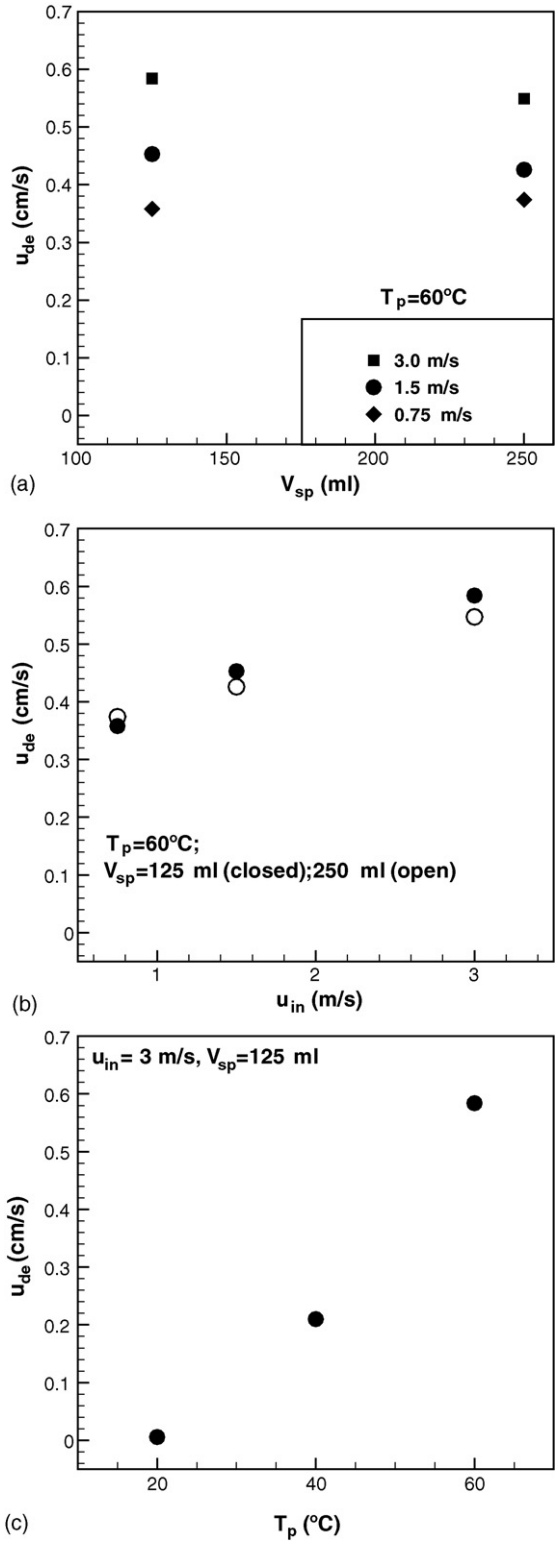

Fig. 7. Rate of decrease in spill size, u_{de}, as a function of (a) spill volume, (b) free stream speed and (c) plate temperature. Other variables held constant as indicated.

A strong dependence of u_{de} on plate temperature is shown in Fig. 7(c). As the temperature rose above the boiling point of acetone, there was over an order of magnitude increase in the regression rate when compared to the 20 °C result. Although no noticeable bubble formation was observed, gas-phase mass

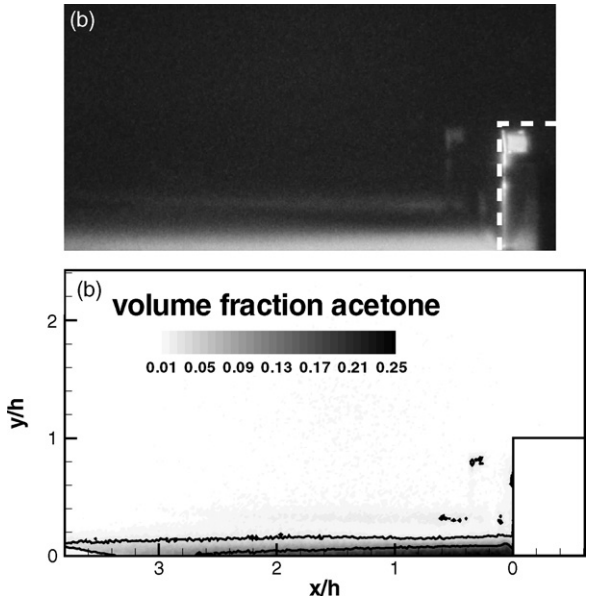

Fig. 8. Instantaneous concentration (a) image with nonlinear scaling to highlight regions of low concentration and (b) PLIF measurement for a 125 ml spill with no wind. $T_p = 20\,^{\circ}C$.

transfer limitations were diminished when the saturation pressure of the fuel rose above atmospheric pressure. This result indicated that spills of cryogenically cooled liquids may likely not be influenced by mass transfer limitations due to the large difference between expected surface temperatures and liquid boiling temperature as suggested elsewhere [6].

The time of maximum spill size, t_{max}, as a function of the experimental parameters is shown in Fig. 9. The time at maximum spill size increased by 55% when the spill volume was doubled, Fig. 9(a). The observation can be explained by the lateral spread of the spill and was consistent with the maximum spill size data shown in Fig. 6(a) as previously discussed. The free stream speed had a significant effect on t_{max}, decreasing it by a factor of 4 when going from 0.75 to 3.0 m/s. The rate of decrease in the time appeared to slow and may reach an asymptotic value at higher wind speeds. The argument for this decrease is explained by the trend in the rate of decrease in the spill size as illustrated in Fig. 7(b). The most striking change in t_{max} occurs by changing the plate temperature, Fig. 9(c). The change in t_{max} was nominally an order of magnitude larger between the 25 and 60 °C plate temperature (62 s versus 3 s) with the trend asymptotically approaching a time near to 0 as expected.

3.2. Cloud formation

Fig. 10 shows a series of instantaneous concentration measurements for which the experimental conditions were: $u_{in} = 3.0$ m/s; $T_p = 60\,^{\circ}C$; $V_{sp} = 250$ ml. The contour levels are bounded by the flammability limits of acetone (2.5–12.8%). The spill began at approximately 0.5 s after the experiment started and continued for nominally 9 s. Concentration measurements were made for an additional 45 s after the spill was completed. During the time of the active spill, the liquid pool expanded downstream, away from the flow obstruction as shown in Fig. 3.

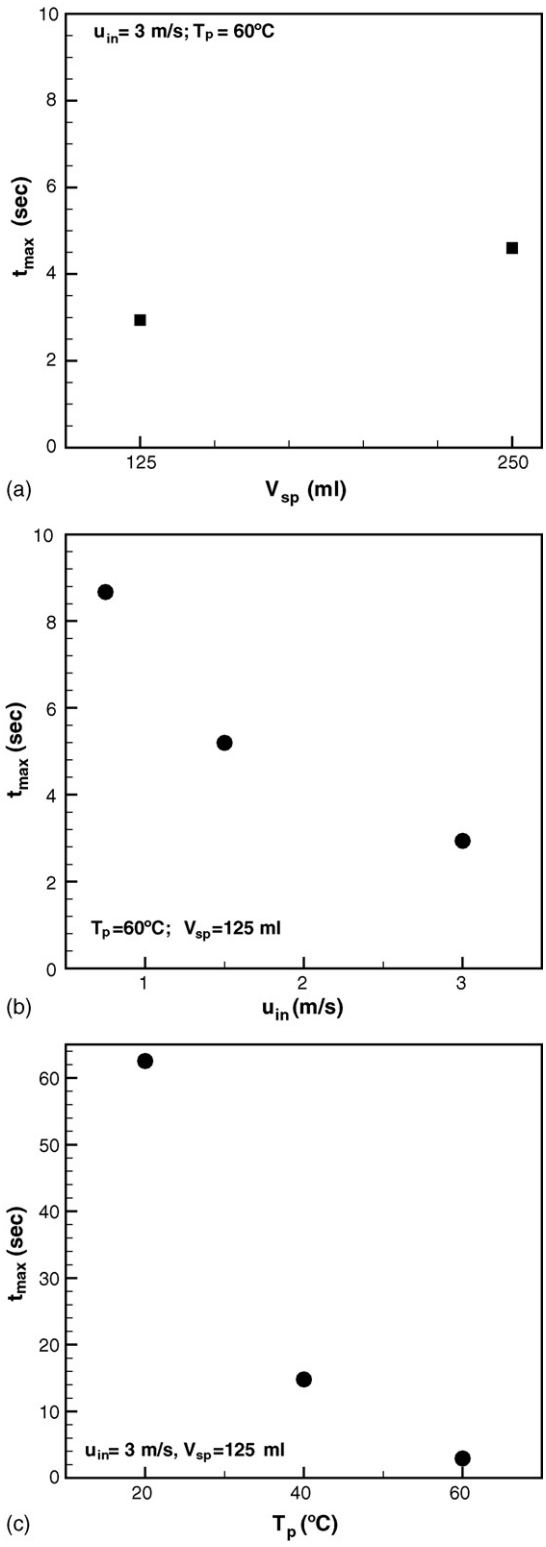

Fig. 9. Time of maximum spill size, t_{max}, as a function of (a) spill volume, (b) free stream speed and (c) plate temperature. Other variables held constant as indicated. Note the change in y-axis range for the plate temperature (c).

Initial acetone vapor was confined to a localized region just downstream of the obstruction, $t < 3.5$ s. The concentrations of acetone vapor were relatively high (i.e. at or near the maximum acetone concentration level). The image shown for $t = 3.5$ s shows the initial indication of acetone vapor above the flow obstruction. As the post-spill and evaporation event continued (i.e. for $t \geq 9.5$ s) the acetone vapor spread both further downstream of the model as well as above the model obstruction. High concentrations of acetone vapor were found near the plate surface, however large regions of acetone vapor within the lean and rich flammability limits (2.5 and 12.8% by volume, respectively) extended from the model downstream out of the measurement domain. It is instructive to note the irregularity of the shape of the flammable regions which will affect the combustion of the vapor.

As discussed in Section 1, the model obstruction caused a large downstream recirculation region. The PLIF images, when viewed in sequence, clearly showed this recirculation, with a counter clock wise direction, downstream of the model. The recirculation region is shown schematically in the $t = 0.5$ s of Fig. 10 for clarity. The flow was directed upstream toward the model along the plate then vertically up the model surface away from the plate. The acetone vapor then was entrained into the separated flow and convected downstream of the obstruction. The shedding caused by the obstruction was also clearly indicated in the PLIF images (e.g. $t = 19.5$ s, $x/h \approx 1.5$). The case illustrated in Fig. 10 showed strong three dimensionality driving motion into and out of the plane. Evidence for this was the observation of large regions of high acetone concentration that appeared above the plate and that did not originate at the plate surface. These observations indicated the presence of large-scale turbulence in the flow field that transported the acetone vapor in three spatial dimensions. Smaller scale turbulence was illustrated by the fine small scale structures shown by the PLIF images as well. Fig. 10 ($t = 9.5$ s) highlights the wide spread, though relatively low concentration, acetone plume extending well past the downstream extent of the measurement domain. This figure also indicated that there was some transport of acetone vapor upstream along the top surface of the obstruction though the concentration of this region was again below the lower flammability limit.

The mass of vaporized acetone along the central plane is shown in Fig. 11 as a function of time and flow speed. While this is not indicative of the total flammable mass of the three-dimensional flow field, it is expected to be indicative of that mass and furthermore to provide a basis for validating complex spill vaporization models to be developed. The maximum mass of acetone vapor in the central plane decreased with increasing wind speed. Furthermore, the lowest positive flow speed investigated, $u_{in} = 0.75$ m/s, also sustained the in-flow flammable mass for the longest period of time of the three wind speeds investigated. The total mass of acetone vapor in the flow field is shown in comparison the flammable mass for $u_{in} = 0.75$ m/s, Fig. 11(b). These data include both concentrations above and below the flammability limits and highlight the significant amount of vapor (~33%) that is ready for rapid premixed combustion or explosion. Fig. 12 shows the flammable mass of acetone as a function of the plate temperature, T_p for $u_{in} = 3.0$ and 0.75 m/s. The mass of acetone within the flammability limits decreased with decreasing plate temperature. This was consistent with the decreased vaporization rate discussed in Section 3.1 for plate temperatures below the acetone boiling point.

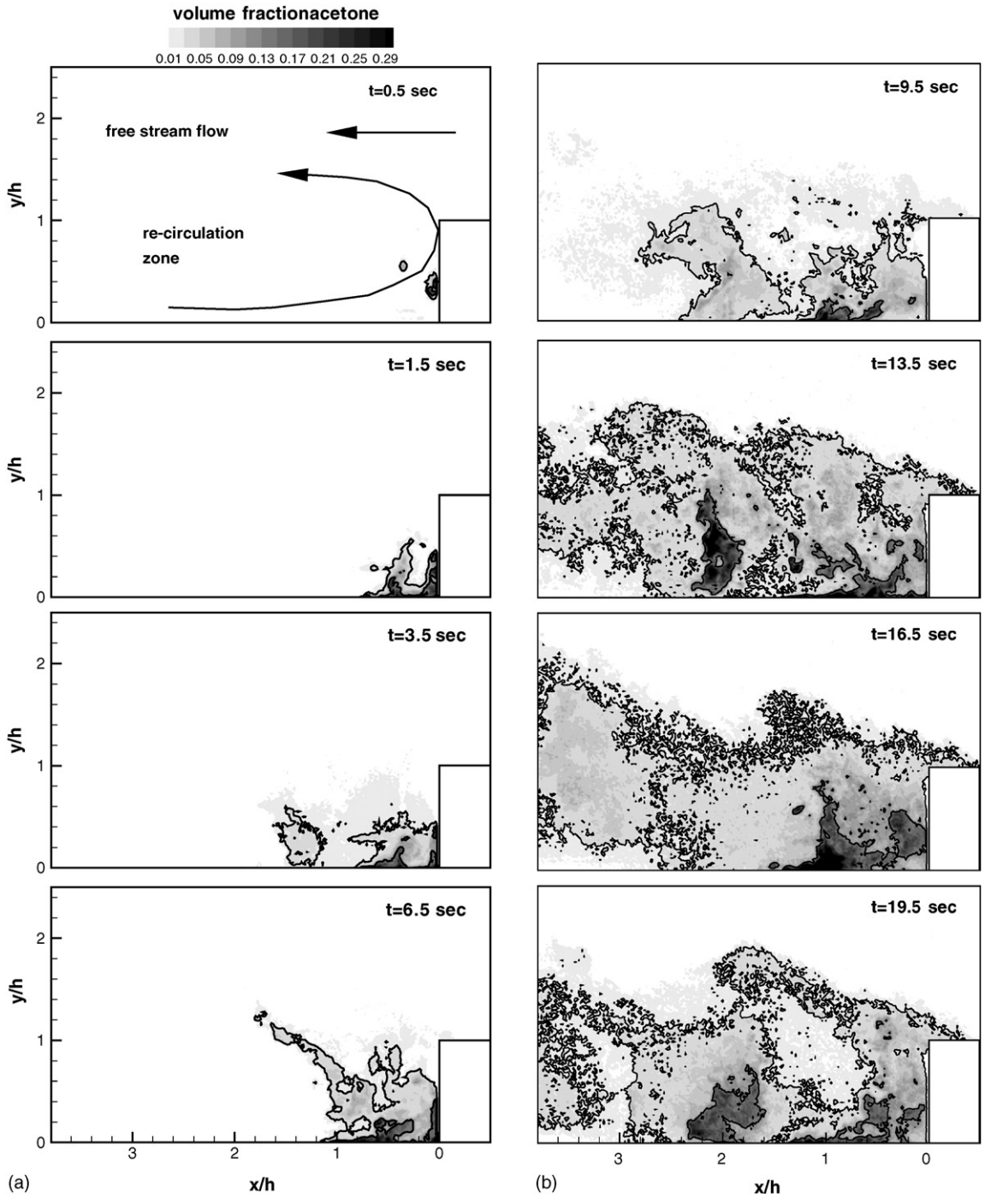

Fig. 10. Instantaneous concentration measurements downstream of the model obstruction. $u_{in} = 3.0$ m/s; $T_p = 60\,^{\circ}$C; $V_{sp} = 250$ ml. Acetone was spilled from $t = 0.5$–9.5 s. Contours indicate volume fraction of acetone. Flammability limits (2.5–12.8%) shown by solid contour lines.

Mean and fluctuating concentration levels were calculated to quantify the turbulence levels in the flow, Fig. 13. Two hundred instantaneous concentration fields after the spill had completed (i.e. during the second and third phase of the experiment) were used to determine the mean and fluctuating concentration fields. The mean data indicated that for each of the cases investigated there existed, a large region in the flow field within the rich and lean flammability limits (2.5–12.8% by volume) downstream of the flow obstruction. The highest concentration levels were located within $3h$ downstream of the obstruction, but the peak concentration region did move upstream toward the obstruction as the wind speed was increased. Fluctuating RMS concentrations were very close in magnitude to the mean levels which indicated the turbulence level was high in the recirculating region of the flow field. The high RMS levels also indicate that at any given instant the required conditions for deflagration/detonation event at a particular spatial location may or may not be met. However, at any given instant, regions within the flammabil-

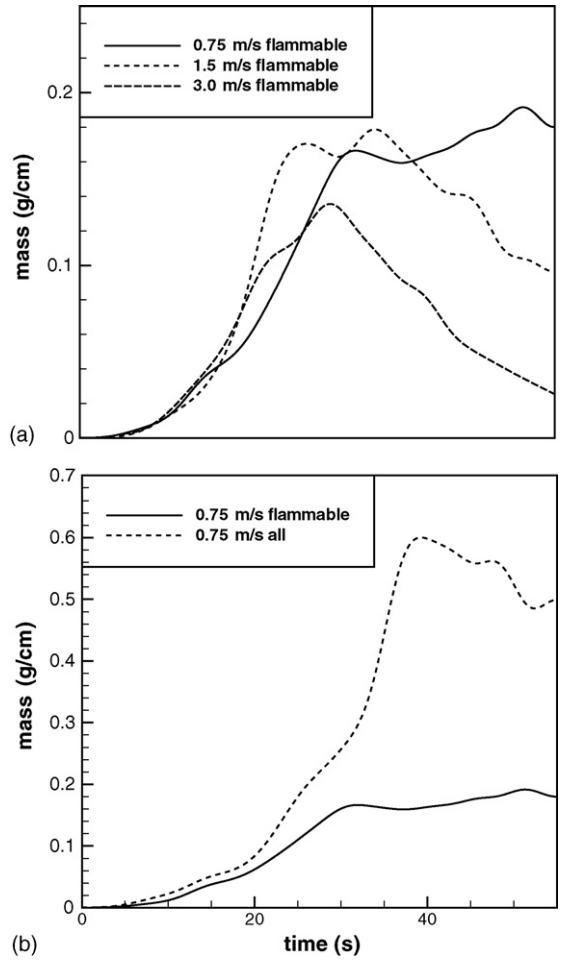

Fig. 11. Integrated acetone mass within the measurement domain as a function of time. (a) Mass within the flammability limits. (b) Total mass of acetone. $T_p = 60\,^{\circ}C$; $V_{sp} = 250$ ml. Speeds as indicated in legend. Note different scales for (a) and (b).

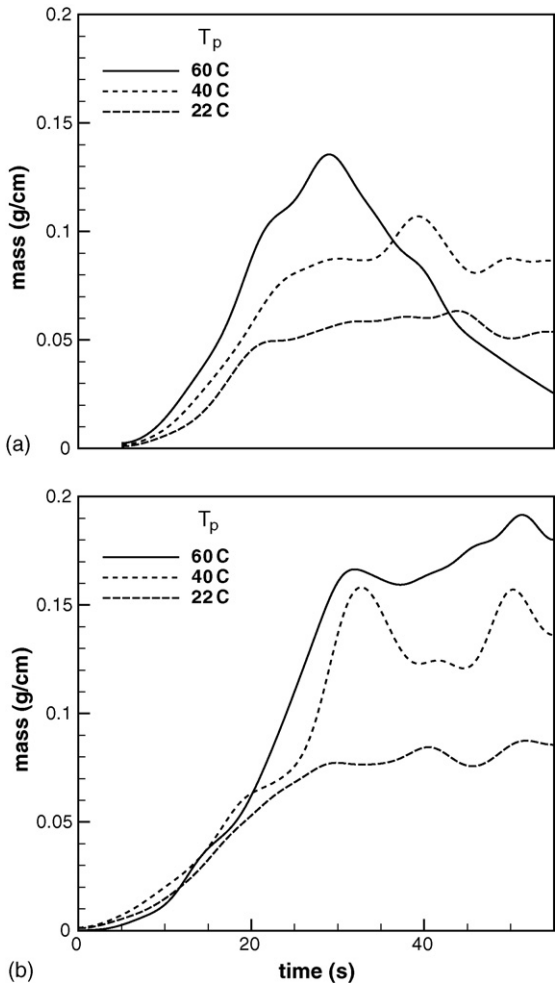

Fig. 12. Flammable acetone mass within the measurement domain as a function of time with (a) $u_{in} = 3.0$ m/s and (b) $u_{in} = 0.75$ m/s. $V_{sp} = 250$ ml. Plate temperature as indicated in legend.

ity limits exist throughout the majority of the visualized vapor cloud. The size and shape of these regions varies from instant to instant and extend well downstream of the flow obstruction beyond the measurement domain (i.e. $x > 3.5h$ downstream of the obstruction).

3.3. Effect of wind speed

The risk of a potentially hazardous explosion of vaporized fuel from a spill is increased with an increase in time that a flammable mixture exists in the flow field. The results of this study indicate that the wind speed plays a significant contributing factor to this hazard level. For the experiments in this study, the concentration of vaporized acetone in the flow field is controlled by both the vaporization rate and the gas-phase flow field. The results indicated that when there was no flow the vaporization was limited by the vapor pressure of acetone and by the diffusion of acetone into the surrounding air, Fig. 8. Within the time scales of the experiment for the still wind case (<15 s), the acetone vapor was limited to a relatively thin region above the spill. Most of the vapor in this spill case was outside of the flammability limits.

When there was a flow present the vaporization increased with a trend towards increased vaporization rate with increasing flow speed. Evidence for this came from the spill images which indicated a decreased spill event time with increasing wind speed, Figs. 7(b) and 9(b). As discussed previously the flow obstruction created a large-scale recirculation region within the flow field. This recirculating flow inhibited the downstream transport of the vaporized acetone and created a region, relatively close to the flow obstruction, in which the acetone vapor could accumulate. Within this region the acetone concentrations were within the flammability limits. The flammable mass calculations presented in Fig. 11 were instructive in determining the most potentially hazardous scenario investigated. The data in Fig. 11(a) support the observation that increasing the wind speed increased the vaporization rate as previously discussed. However, it was also clear from these data that the increased wind speed decreased the amount of flammable mass in the recirculation region and the time of high concentrations after the spill. The lower wind speed decreased the vaporization rate, however, the flow field induced by this wind created a situation with higher total flammable mass and a longer total event time. This difference was most probably due to increased down-

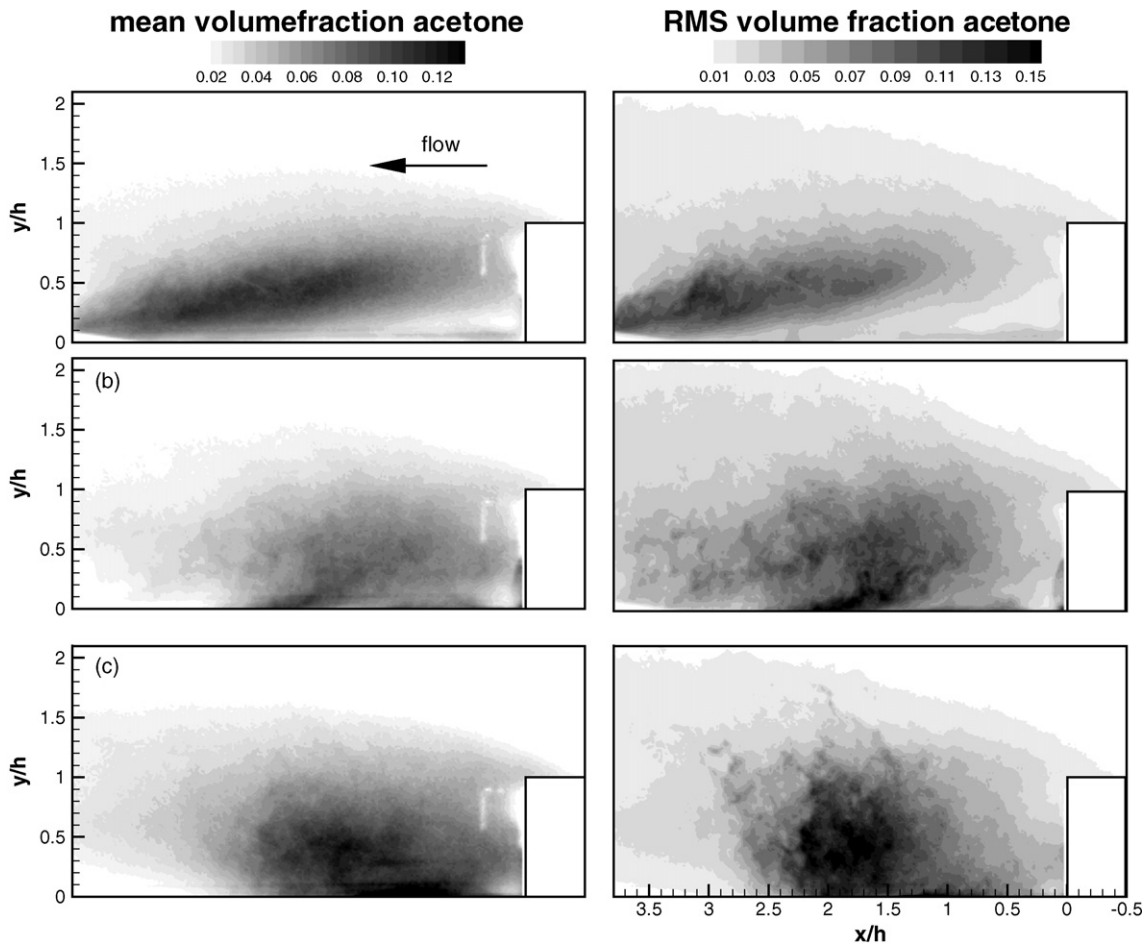

Fig. 13. Mean and rms fluctuating acetone concentration for (a) $u_{in} = 0.75$ m/s, (b) $u_{in} = 1.5$ m/s and (c) $u_{in} = 3.0$ m/s. $T_p = 60\,^{\circ}$C; $V_{sp} = 250$ ml. Flow right to left as shown in (a).

stream convection for the higher wind speed. These observations indicate that there is a complex functional dependence of the hazard level on the wind speed and that there appears to be a wind speed that poses an optimum hazard. This speed, which appears to be relatively low for the cases investigated here, represents a trade-off between vaporization rate and convection rate.

4. Conclusions

In this work the spill of a volatile liquid, acetone, onto a heated surface downstream of a large obstruction in a flow field was investigated. The obstruction, a rectangular obstruction that spanned the width of the tunnel, was oriented perpendicular to the free stream wind speed. The experiments were intended to be a first order simulation of the spill of a volatile flammable liquid from a large transport vessel onto a non-porous or a smooth water surface and the resulting vapor cloud. Experimental conditions, plate temperature, approach wind speed and spill volume were varied with temperatures below and above the boiling point of the liquid acetone. The highest temperature was 4 °C above the boiling point of acetone. Variations in wind speeds (up to 3.0 m/s) showed the critical importance of wind speed in assessing the variation in flammable mass in the vapor cloud with spill variation. Contrary to some existing spill models, the coupling between the gas flow field and the liquid spill may be very important in determining the extent of the spill spreading and the overall spill shape. A spill downstream of a large flow obstruction is particularly influenced by the strong recirculation zone, which tends to capture some of the fuel mass for enough time to build up a flammable mass.

Digital video images to characterize the spill process showed that the maximum spill size increased with the spill volume at constant surface temperature and decreased with increasing surface temperature at constant spill volume. No dependence of the maximum spill size was shown with the free stream speed for the limited range of velocities tested in this study ($\leq$3.0 m/s), although it is not clear that such independence of spill size would apply at higher free stream speeds or for other geometries. On the other hand, the decrease in spill size due to the evaporation rate was shown to be a function of the free stream speed and plate temperature but not total spill volume.

The results of the PLIF data showed that as the acetone vaporization and subsequent cloud formation was controlled by the recirculating flow downstream of the flow obstruction. Acetone vaporized at the bottom surface of the tunnel and was convected upstream towards the flow obstruction by the recirculating flow. The acetone vapor then followed the downwind side of the

obstruction up away from the tunnel floor and into the overheated flow field. Large-scale shedding patterns were observed on the edge of the acetone vapor cloud. Turbulent motion, both large scale and small scale, was observed in the recirculation region. Fluctuating concentration values, nearly equal to the mean values, were observed indicating the strength of the turbulent motions in this flow field. There were areas within the flammability limits downstream of the flow obstruction that extended well past the downstream edge of the measurement domain.

The dynamics of the vaporization and convection processes are such that the most potentially hazardous scenario represents a trade-off between vaporization rate and convection speed. The results of this work indicate that the lowest non-zero wind speed investigated poses the most significant risk in that both the amount of flammable material and the event time were maximized for this case. The current results provide a data set which may be used for future spill model developers to couple complex CFD calculations with spill models that incorporate the critical coupling between the gas-phase flow and the spill spreading and vaporization. For the range of conditions tested, such models may prove useful in predicting the behavior of similar physical processes at much larger scales where hazardous risk assessment is critical for evaluating safe transport of flammable liquid materials.

Acknowledgements

This work was supported by the Port Security Project at the Office of Naval Intelligence and conducted at the Naval Surface Warfare Center Indian Head Division in Indian Head Maryland. The authors would like to thank Todd Stevens, Ronak Patel, and Robert Hay for their support in the development and execution of the experiments.

References

[1] J.A. Fay, Risks of LNG and LPG, Annu. Rev. Energy 5 (1980) 89–105.
[2] D.A. Crowl, Understanding Explosions, Center for Process Safety of the American Institute of Chemical Engineers, New York, 2003.
[3] J.A. Fay, Unusual fire hazard of LNG tanker spills, Combust. Sci. Technol. 7 (2) (1973) 47–49.
[4] F. Briscoe, P. Shaw, Spread and evaporation of liquid, Prog. Energy Combust. Sci. 6 (2) (1980) 127–140.
[5] J.A. Fay, Model of spills and fires from LNG and oil tankers, J. Hazard. Mater. 96 (2/3) (2003) 171–188.
[6] C. Conrado, V. Vesovic, The influence of chemical composition on vaporisation of LNG and LPG on unconfined water surfaces, Chem. Eng. Sci. 55 (20) (2000) 4549–4562.
[7] T.O. Spicer, J.A. Havens, Application of dispersion models to flammable cloud analyses, J. Hazard. Mater. 49 (2/3) (1996) 115–124.
[8] A. Evans, J.S. Puttock, Experiments on the ignition of dense flammable gas clouds, in: Proceedings of the International Symposium on Loss Prevention and Safety Promotion in the Process Industries, Cannes, September, 1986.
[9] J.A. Havens, T.O. Spicer, LNG vapor cloud exclusion zones for spills into impoundments, Process Saf. Prog. 24 (3) (2000) 181–186.
[10] Y. Addad, D. Laurence, C. Talotte, M.C. Jacob, Large eddy simulation of a forward–backward facing step for acoustic source identification, Int. J. Heat Fluid Flow 24 (4) (2003) 562–571.
[11] D. Leclercq, M. Jacob, A. Louistot, C. Talotte, Forward backward facing step pair: aerodynamic flow, wall pressure and acoustic characterization, AIAA Paper 2001-2249, 2001.
[12] A. Lozano, B. Yip, R.K. Hanson, Acetone—a tracer for concentration measurements in gaseous flows by planar laser-induced fluorescence, Exp. Fluids 13 (6) (1992) 369–376.
[13] I. Vancruyningen, A. Lozano, R.K. Hanson, Quantitative imaging of concentration by planar laser-induced fluorescence, Exp. Fluids 10 (1) (1990) 41–49.